Salient features of scattering amplitudes in intermediate energy nucleon-nucleus scattering

P. Susan and C. S. Shastry
Physics Department, North Eastern Hill University, Shillong-793 003, India

Y. K. Gambhir
Physics Department, Indian Institute of Technology, Powai, Bombay-400 076, India
(Received 28 April 1994)

Phenomenological relativistic optical models for scattering of nucleons from a spin-0 nucleus mainly use two different approaches. In the first, one essentially uses the Schrödinger equation incorporating appropriate relativistic kinematical terms. In the second approach, which is superior especially in reproducing spin observables, one starts with the Dirac equation and obtains an equivalent Schrödinger equation which forms a convenient basis for the calculation of experimental observables. Adopting a mathematical procedure developed earlier within the framework of potential scattering, we calculate the regionwise contribution to the reaction cross section for spin-$\frac{1}{2}$–spin-0 systems using both these types of relativistic optical models. The relative importance of different regions of intermediate energy optical potential in generating the total reaction cross section is examined using the method of regionwise absorption and it is found that reaction process is surface dominant. These findings are further elaborated by depicting the general features of S matrix and scattering amplitudes as a function of angular momentum.

PACS number(s): 24.10.Ht, 24.10.Jv, 25.40.Cm

I. INTRODUCTION

During the last few decades medium energy nucleon-nucleus scattering has been an area of much interest [1–9], especially in view of the accumulation of detailed experimental results on differential cross section, analyzing power, and the spin rotation function obtained by using polarized beams. A simple approach for the analysis of the data is to use the conventional Schrödinger equation with relativistic kinematics (RK) built in, in order to generate the correct de Broglie wavelength and relativistic density of states [10]. However, this approach is found to be inadequate in reproducing spin observables accurately. A more successful approach is to start with the Dirac equation with appropriate inputs, i.e., vector and scalar potential terms based on relativistic mean field (RMF) theory. In the Dirac phenomenology, which is astonishingly successful in reproducing the spin observables and cross sections, the complex vector and scalar potential terms are usually assumed to be of the Woods-Saxon form, involving a number of adjustable parameters. These input vector and scalar potentials can be obtained microscopically, starting from the basic nucleon-nucleon scattering amplitudes within the framework of relativistic impulse approximation and incorporating the medium and Pauli (exchange) effects. The agreement between the microscopically deduced potentials and the corresponding Dirac phenomenological potentials is remarkable [11–13]. In this paper we use phenomenological complex vector and scalar potentials. The Dirac equation for nucleon-nucleus scattering can be reduced to an equivalent Schrödinger equation to facilitate the calculations [11]. This Dirac-Schrödinger (DS) phenomenology is found to be superior to the RK approach in describing the intermediate energy nucleon-nucleus scattering including the spin observables. This success is attributed to the fact that in the DS approach the correct energy dependence of the effective potential, especially the well-known gradual transition of the real part of the effective potential from the attractive Woods-Saxon form to the wine bottle bottom shape at the transition energies, is properly incorporated. In fact, one can use this approach to obtain global energy-dependent optical potentials [14,15] for the intermediate energy nucleon-nucleus scattering.

Even though the relativistic phenomenological optical potential model with several parameters gives the proper description of the scattering data, the details of the regions of the nucleus which partake in the scattering and reaction processes do not become apparent in such calculations. For example, one can seek information regarding the finer details and differences in the scattering and reaction process involved in the DS and RK approaches. In a set of papers [16,17], two of us have developed a procedure to determine the relative sensitivity of different regions of the potentials in the nuclear reaction processes. This helps to establish the domain of the interaction which is primarily responsible for the generation of the scattering amplitudes. Such an analysis is indeed very useful especially in determining the regions of the nucleus explored by the probe. Here we extend this procedure to the analysis of intermediate energy nucleon-nucleus scattering.

In addition to the above, we study in this paper the angular momentum (l) space behavior of the relevant partial wave amplitudes occurring in the RK and the DS

approaches. Such an analysis of the general properties and structure of the S matrix and scattering amplitudes in l space has not been carried out so far in the case of the relativistic nucleon-nucleus optical model. This, together with the configuration space analysis of the reaction cross section, provides a detailed comparative picture of the DS and RK approaches to the relativistic proton-nucleus optical model. It may be noted that the knowledge of the l dependence of the partial wave amplitudes is also important in the formulation of closed formalism or the parametric S-matrix approach [18–20].

In Sec. II we study and analyze the contribution to the reaction cross section from different regions of the coordinate space by using the RK and DS approaches, with the aim of bringing out the differences in the two approaches and thereby identifying the specific features of the DS approach. In Sec. III we investigate the detailed properties of the S matrix and the amplitudes in the case of RK and DS approaches and determine the regions of angular momentum space which dominate the scattering. Summary and conclusions are contained in Sec. IV.

II. REGIONWISE ABSORPTION IN OPTICAL MODEL

The analysis based on the optical model is the most common method used to study the collision process which has elastic, inelastic, and reaction channels. The nuclear optical model is used to study the nucleon-nucleus and nucleus-nucleus collisions. In addition to elastic scattering, this model describes the absorption or reaction cross section. The imaginary part of the complex potential accounts for the absorption of incident flux leading to reaction cross section $\sigma_{\rm rec}$ generated by all nonelastic channels. In this section we summarize a mathematical approach to calculate the regionwise contribution (in r space) to the $\sigma_{\rm rec}$ for spin-$\frac{1}{2}$–spin-0 systems within the framework of optical model. We also make a comparative study of the same using the RK and DS approaches for p+^{40}Ca scattering at 181 and 362 MeV proton energies.

A. Mathematical formalism

In [16,17] a procedure was formulated to obtain the contribution to the reaction cross section from a shell of radius r and thickness Δ around the scattering center within the framework of the nuclear optical model. Here we summarize the essential and relevant mathematical results appropriately modified for spin-$\frac{1}{2}$–spin-0 systems.

For spin-$\frac{1}{2}$–spin-0 systems the reaction cross section for particles of angular momentum l is given by

$$\sigma_{\rm rec}^{(l)} = \frac{\pi}{k^2}[(l+1)(1-\eta_l^{+2}) + l(1-\eta_l^{-2})], \tag{1}$$

where $\eta_l^{\pm} = |S_l^{\pm}|$. The partial wave S matrix $S_l^{\pm}$ corresponds to $j = l \pm \frac{1}{2}$. The total reaction cross section is given by

$$\sigma_{\rm rec} = \sum_{l=0}^{\infty} \sigma_{\rm rec}^{(l)}. \tag{2}$$

The factor $1-(\eta_l^{\pm})^2$ can be obtained from the regular solution of the Schrödinger equation:

$$\frac{d^2}{dr^2}\Phi^{\pm}(\lambda,k,r) + \left(k^2 - \frac{\lambda^2-1/4}{r^2} - V_{\rm eff}^{\pm}(r) - \frac{2\eta k}{r}\right)\Phi^{\pm}(\lambda,k,r) = 0, \tag{3}$$

where k^2 is the energy, $\lambda = l + \frac{1}{2}$, η is the Coulomb parameter, and $V_{\rm eff}^{\pm}(r)$ is the total effective potential appropriate for $j = l \pm \frac{1}{2}$. It can be shown [16,17] that

$$\begin{aligned} i-(\eta_l^{\pm})^2 &= -4k\int_0^{\infty} U_I(r)\left|\frac{\Phi^{\pm}(\lambda,k,r)}{F^{\pm}(\lambda,-k)}\right|^2 dr \\ &= -4k\int_0^{\infty} U_I(r)\left|\left\{\frac{\Phi^{\pm}(\lambda,k,r)}{F^{\pm}(\lambda,-k)r}\right\}\right|^2 r^2\,dr \\ &= \sum_{i=0}^{\infty}\chi_{\rm rec}^{\pm}(\lambda,r_i,\Delta), \end{aligned}$$

$$r_0 = 0,\ r_{i+1} = r_i + \Delta, \tag{4}$$

where $U_I(r)$ is the imaginary part of the total effective potential. Here $\Phi^{\pm}(\lambda,k,r)$ is the regular solution of (3) which behaves like $r^{\lambda+1/2}$ near the origin and $F^{\pm}(\lambda,-k)$ is the Jost function [21–23]. The second integral involving r^2dr in (4) clarifies the fact that we are expressing $1-(\eta_l^{\pm})^2$ as an integral over the volume in the interaction region. In fact the expression in the curly brackets in (4) is the actual radial part of the full scattering wave function satisfying the scattering wave boundary condition Thus, $\chi_{\rm rec}^{\pm}(\lambda,r_i,\Delta)$ is a measure of the contribution to $\sigma_{\rm rec}^{(l)}$ from the region $r_i \le r \le r_i+\Delta$. $\chi_{\rm rec}^{\pm}$ can be expressed as

$$\chi_{\rm rec}^{\pm}(\lambda,r_i,\Delta) = -4k\,{\rm Im}\left[\frac{\Phi^{\pm\prime}(\lambda,k,r)\phi^{\pm *}(\lambda,k,r)}{F^{\pm}(\lambda,-k)F^{\pm *}(\lambda,-k)}\right]\Bigg|_{r_i}^{r_i+\Delta}. \tag{5}$$

Here the prime denotes the derivative with respect to r. The reaction cross section $\sigma_{\rm rec}(r_i,\Delta)$ generated in the region $r_i \le r \le r_i+\Delta$ is

$$\sigma_{\rm rec}(r_i,\Delta) = \frac{\pi}{k^2}\sum_{l=0}^{\infty}[(l+1)\chi_{\rm rec}^{+}(\lambda,r_i,\Delta) + l\chi_{\rm rec}^{-}(\lambda,r_i,\Delta)]. \tag{6}$$

Further, the contribution to $\sigma_{\rm rec}$ from the region $0 \le r \le r_N$ can be expressed as

$$[\sigma_{\rm rec}]_0^{r_N} = \sum_{i=0}^{N} \sigma_{\rm rec}(r_i, \Delta). \tag{7}$$

$\sigma_{\rm rec}(r_i, \Delta)$ indicates the contribution to $\sigma_{\rm rec}$ from the spherical shell of inner radius r_i and outer radius $r_i + \Delta$ and $[\sigma_{\rm rec}]_0^{r_N}$ is the contribution of the spherical volume of radius r_N around the scattering center to the reaction cross section $\sigma_{\rm rec}$.

In the following we numerically analyze the behavior of $\sigma_{\rm rec}(r_i, \Delta)$ and $[\sigma_{\rm rec}]_0^{r_N}$ for the p+^{40}Ca system at 181 and 362 MeV using both the RK and DS approaches.

B. Numerical calculations

In the RK approach, relativistic kinematics [10] are incorporated into the conventional Schrödinger equation. In this approach we have used the correct relativistic momentum

$$k = \frac{M}{\hbar c}\left[\frac{E_L(E_L+2m)}{(m+M)^2+2ME_L}\right]^{1/2}, \tag{8}$$

where m and M are the rest masses of the nucleon and the nucleus, respectively. E_L is the nucleon kinetic energy in the laboratory frame. The optical potential has a complex central part with the Woods-Saxon form, the complex spin orbit part having a derivative of the Woods-Saxon form to which is added the Coulomb potential from a uniformly charged sphere of radius R_C.

In the DS approach the complex input potential consists of $U_v(r)$, which transforms like the timelike component of a Lorentz four-vector, and $U_s(r)$, which is a Lorentz scalar. The Dirac equation with these potentials is

$$\{\alpha \cdot p + \beta[m + U_s(r)] + [U_v(r) + V_C(r)]\}\Psi(r) = E\Psi(r). \tag{9}$$

Here $V_C(r)$ is the Coulomb potential and E is the nucleon total energy in the center of mass frame.

The complex potentials $U_s(r)$ and $U_v(r)$ are taken to be of the form

$$U_i(r) = V_i f_i(r) + iW_i g_i(r), \quad i = s, v\ , \tag{10}$$

where $f_i(r)$ and $g_i(r)$ are of the form $\{1 + \exp[(r_i - c_i)/a_i]\}^{-1}$. The equivalent Dirac-Schrödinger equation becomes

$$\left\{\frac{d^2}{dr^2} + k^2 - \left[V_{\rm cent}(r) + \begin{pmatrix} l \\ -l-1 \end{pmatrix} V_{\rm S.O.}(r) + V_{\rm Darwin}\right] - \frac{l(l+1)}{r^2}\right\}\Psi^{\pm}(r) = 0, \tag{11}$$

where

$$V_{\rm cent}(r) = 2mU_s(r) + 2EU_v(r) + U_s^2(r) - U_v^2(r) - 2V_C U_V(r), \tag{12}$$

$$V_{\rm Darwin} = \frac{3}{4}\left(\frac{B'}{B}\right)^2 - \frac{1}{r}\frac{B'}{B} - \frac{1}{2}\frac{B''}{B}, \tag{13}$$

where

$$B = \frac{E + m + U_s(r) - U_v(r)}{E + m}, \tag{14}$$

$$V_{\rm SO}(r) = -\frac{1}{r}\frac{B'}{B}, \tag{15}$$

and the prime denotes the derivative with respect to r.

Using the expressions listed in Sec. II A, we study the nature of the absorption in the case of a typical proton-nucleus system, i.e., p+^{40}Ca at 181 and 362 MeV. This choice of energy range 181–362 MeV covers the transition energy region where the real part of the effective central potential changes from the attractive wine bottle bottom shape to repulsive Woods-Saxon-type form [11–13]. The least squares fitted potential parameters used in the analysis, taken from [1,2], are listed in Table I. The value of R_C used is $1.25A^{1/3}$. We have analyzed the behavior of $[\sigma_{\rm rec}]_0^{r_N}$ and $\sigma_{\rm rec}(r_i, \Delta)$ using both the RK and DS approaches. We also studied the radial variation of $\chi_{\rm rec}^{\pm}(\lambda, r_i, \Delta)$ for different partial waves l which gives the contribution to $(1 - \eta_l^{\pm 2})$ from the region $(r_i, r_i + \Delta)$.

In Figs. 1 and 2 we illustrate the variation of $[\sigma_{\rm rec}]_0^{r_N}$ and $\sigma_{\rm rec}(r_i, \Delta)$ as a function of r in the case of p+^{40}Ca at 181 and 362 MeV, respectively, for both the RK and DS approaches. As is evident from the figures, $\sigma_{\rm rec}(r_i, \Delta)$ is peaked around the surface region of the target nucleus, indicating that maximum absorption occurs at the surface region. The maximum slope of $[\sigma_{\rm rec}]_0^{r_N}$ as a function of r occurs when $\sigma_{\rm rec}(r_i, \Delta)$ is maximum. $[\sigma_{\rm rec}]_0^{r_N}$ saturates to the value $\sigma_{\rm rec}$ (the reaction cross section) as r becomes large, implying negligible absorption in the region further exterior. From these results it is also clear that irrespective of whether one uses the RK or DS approach with volume absorptive imaginary potential, the reaction process in the intermediate energy relativistic proton-nucleus scattering is surface dominant. It may be pointed out here that these results differ considerably from the results obtained in the analysis of regionwise absorption of the flux in the low energy (5–20 MeV) neutron-nucleus and proton-nucleus scattering using volume absorptive imaginary part of the optical potential. It was found that in the low energy cases the volume absorptive optical potential generates absorption in more or less the entire volume of the nucleus [17]. The regionwise absorption pattern in the relativistic collision shows very striking similarity with the absorption process in heavy ion scattering [16], leading to the conclusion that surface

TABLE I. Phenomenological optical potential parameters for the p+^{40}Ca system.

E_L (MeV)	Potential	Strength (MeV)	Radius (fm)	Diffuseness (fm)	Reference
	(a) RK Phenomenological optical potential				
181	Central $U_{\rm cent}$	−17.3	4.310	0.780	[1]
	Central $W_{\rm cent}$	−8.7	4.326	0.645	[1]
	Spin orbit $U_{\rm SO}$	−2.83	3.523	0.610	[1]
	Spin orbit $W_{\rm SO}$	1.85	3.523	0.610	[1]
362	Central $U_{\rm cent}$	14.9	2.209	0.515	[2]
	Central $W_{\rm cent}$	−34.5	3.793	0.681	[2]
	Spin orbit $U_{\rm SO}$	−3.86	3.440	0.703	[2]
	Spin orbit $W_{\rm SO}$	4.342	3.410	0.703	[2]
	(b) DS Phenomenological optical potential				
181	Vector U_v	334	3.474	0.668	[1]
	Vector W_v	−107	3.487	0.716	[1]
	Scalar U_s	−437	3.453	0.692	[1]
	Scalar W_s	109	3.453	0.692	[1]
362	Vector U_v	294.6	3.454	0.64	[2]
	Vector W_v	−97	3.830	0.55	[2]
	Scalar U_s	−419.9	3.420	0.67	[2]
	Scalar W_s	99	3.830	0.54	[2]

dominance of the physical process is an important feature of relativistic intermediate energy nucleon-nucleus scattering.

The results discussed above are in the context of overall cumulative effect of all relevant partial waves. Hence the above conclusions do not preclude the possibility of the inner region being sensitive for some partial waves. In the reaction cross section, the higher partial wave contribution naturally gets enhanced significantly due to the $l+1$ and l multiplying factor. To illustrate this point we show the radial variation of $\chi^{+}_{\rm rec}(\lambda, r_i, \Delta)$ in the case of p+^{40}Ca at 181 and 362 MeV for three relevant partial waves in Figs. 3(a) and 3(b). Similar behavior is observed for $\chi^{-}_{\rm rec}(\lambda, r_i, \Delta)$ also.

From the above-noted figures it is clear that the regionwise absorption pattern generated by RK and DS is qualitatively similar even though there are some significant quantitative differences. It is found by earlier workers [1] that this quantitative difference is due to the large difference in the strength of the imaginary effective potential used in the above approaches. Needless to say, it is such differences which may be leading to the superiority of DS in explaining the experimental observables. More features of the amplitudes in the case of DS are discussed in the following section.

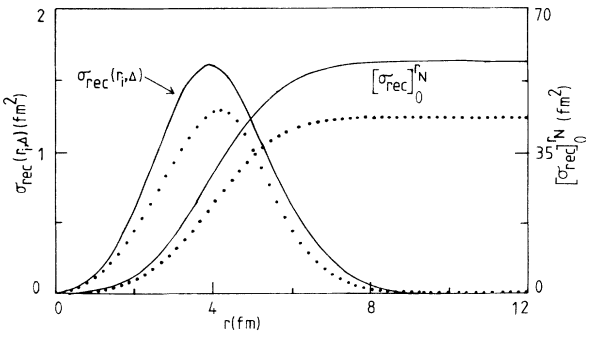

FIG. 1. Variation of $\sigma_{\rm rec}(r,\Delta)$ and $[\sigma_{\rm rec}]_0^{rN}$ as a function of r for p+^{40}Ca scattering at E_L = 181 MeV. The solid and dotted lines indicate the results obtained by the DS and RK approaches, respectively. The optical potential parameters used in the calculation are listed in Table I. Here Δ = 0.1 fm.

III. VARIATION OF THE S MATRIX AND PARTIAL WAVE AMPLITUDES WITH l

The physical picture of scattering can be understood from the properties of scattering matrix. Hence in this section we investigate the detailed properties of S ma-

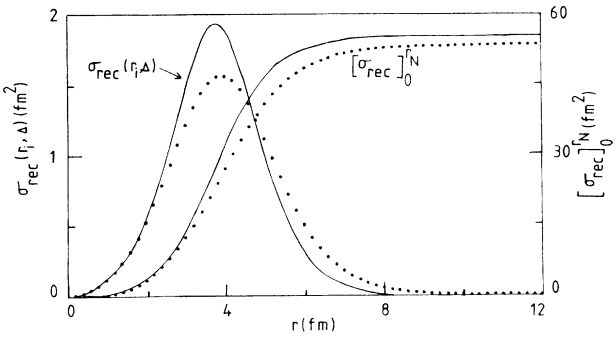

FIG. 2. Same as in Fig. 1 for p+^{40}Ca at E_L = 362 MeV.

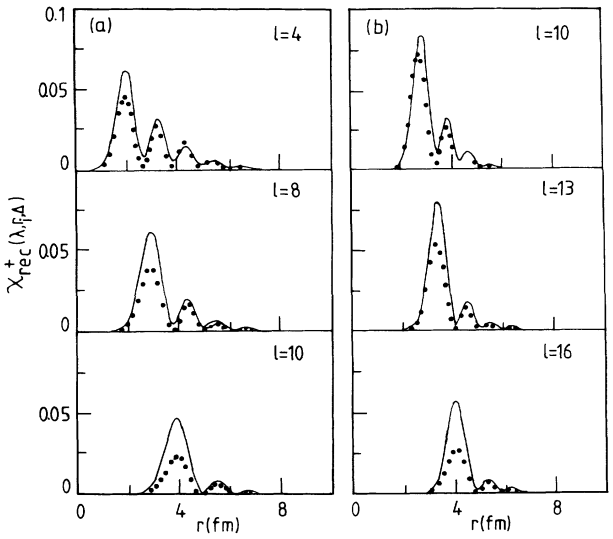

FIG. 3. Radial variation of $\chi^{+}_{\rm rec}(\lambda, r, \Delta)$, giving the contribution to $[1-\eta_l^{+2}]$. (a) p+^{40}Ca at 181 MeV for $l = 4$, 8, and 10 and (b) p+^{40}Ca at 362 MeV for $l = 10$, 13, and 16. For other details see Fig. 1 caption.

trix and scattering amplitudes in the case of medium energy nucleon-nucleus scattering. From the structure of the scattering amplitudes we extract the main features of the relativistic optical model and the subtle differences between the RK and DS approaches.

A. Scattering matrix

The behavior of the S matrix as a function of l is important in understanding the details of the physical processes involved in the RK and DS approaches. Figures 4(a) and 4(b) show the variation of $|S_l^{\pm}|$ as a function of l obtained from both DS and RK approaches. It is clear that $|S_l^{\pm}|$ has smooth variation as a function of l approaching unity in both the DS and RK approaches. The functional dependence of $|S_l^{\pm}|$ is akin to the corresponding result in heavy ion scattering as far as the smooth Fermi-function-type behavior is concerned. However, there are some important differences. It is known that in heavy ion collisions most of the partial waves $l < l_g$ [$\simeq kR(1-2\eta/kR)^{1/2}$, $R = r_0 A^{1/3}$] the grazing partial waves are almost fully absorbed ($|S_l^{\pm}| = 0$), whereas in the present case where $l_g \simeq kR$ due to small η there is a significant nonzero value of the magnitude of the S matrix even for lower partial waves even though surface dominance is approximately the same as in heavy ion scattering. The rise of $|S_l^{\pm}|$ to unity is faster in heavy ion scattering. This implies that the surface thickness explored in intermediate energy proton-nucleus collisions is broader. It may be remarked that it is also a common practice in heavy ion physics to define l_g using the definition $|S_{lg}| = 0.5$. Since values of l_g obtained from $|S_l^{+}|$ and $|S_l^{-}|$ are not found to be the same, in general, we restrict ourselves to the definition of l_g stated earlier with parameter $r_0 = 1.1$ fm. From these figures it is also

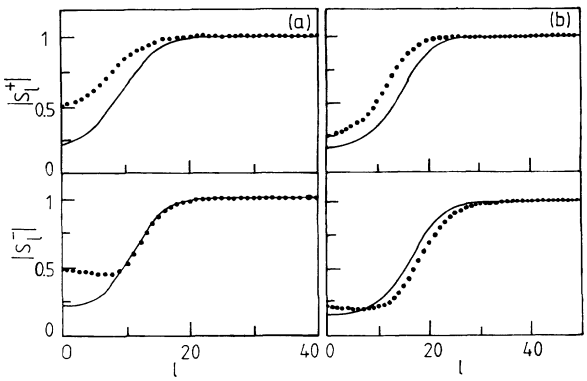

FIG. 4. Variation of $|S_l^{\pm}|$ as a function of orbital angular momentum l. (a) p+^{40}Ca at $E_L = 181$ MeV, $l_g = 11$ and (b) p+^{40}Ca at 362 MeV, $l_g = 16$. For other details see Fig. 1 caption.

evident that there is a substantial difference in $|S_l^{\pm}|$ for the interior partial waves, i.e., approximately for $l < l_g$. It is also clear that for $l < l_g$ the DS model is much more absorptive than the RK model.

Unlike the case in $|S_l^{\pm}|$ the variations of phase shift $\delta_l^{\pm}$ [Figs. 5(a) and 5(b)] obtained using the RK and DS approaches are significantly different. Perhaps it is this difference which is responsible for the better reproduction of experimental observables by the DS approach. Further, the comparison of Figs. 5(a) and 5(b) shows that variation of $\delta_l^{\pm}$ is also strongly energy dependent. The well-established gradual change from the attractive to repulsive character of the effective potential as a function of energy is responsible for this dissimilar behavior of the phase shift.

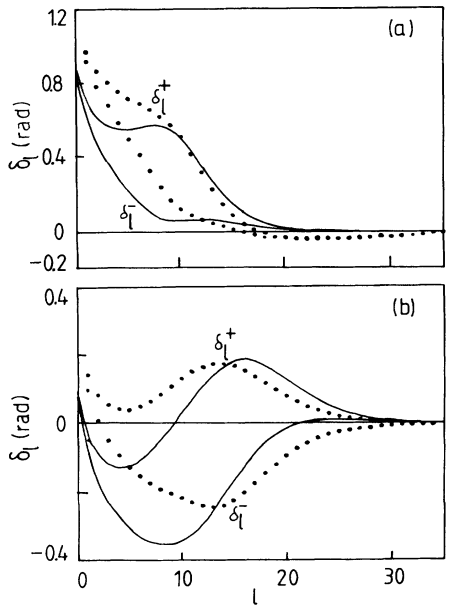

FIG. 5. Variation of $\delta_l^{\pm}$ as a function of l. (a) p+^{40}Ca at $E_L = 181$ MeV and (b) p+^{40}Ca at 362 MeV. For other details see Fig. 1 caption.

B. Scattering amplitudes

Even though the differential cross section is well reproduced by both the RK and DS approaches [1,5] there is a remarkable difference in the spin observables obtained from these two approaches. The explicit expressions for the differential cross section $\sigma(\theta)$ in the case of unpolarized incident beam and the corresponding spin observables, namely, the analyzing power $A_y(\theta)$ and spin rotation function $Q_y(\theta)$ are

$$\sigma(\theta) = |A(\theta)|^2 + |B(\theta)|^2, \tag{16}$$

$$A_y(\theta) = \frac{2\,\mathrm{Re}A^*(\theta)B(\theta)}{\sigma(\theta)}, \tag{17}$$

$$Q_y(\theta) = \frac{2\,\mathrm{Im}A(\theta)B^*(\theta)}{\sigma(\theta)}. \tag{18}$$

The scattering amplitudes $A(\theta)$ and $B(\theta)$ are obtained from the following expressions

$$A(\theta) = f_c(\theta) + \frac{1}{2ik}\sum_{l=0}^{\infty}\exp(2i\sigma_l)[(l+1)S_l^+ + lS_l^- - (2l+1)]P_l(\cos\theta), \tag{19}$$

where $f_c(\theta)$ and σ_l are the Coulomb scattering amplitude and phase shifts, respectively,

$$B(\theta) = i\frac{1}{2ik}\sum_{l=0}^{\infty}\exp(2i\sigma_l)[S_l^+ - S_l^-]P_l^1(\cos\theta). \tag{20}$$

The expression for spin observables involves factors such as $\mathrm{Re}[A^*(\theta)B(\theta)]$ and $\mathrm{Im}[A(\theta)B^*(\theta)]$. Therefore it is interesting to study the variation of the partial wave contribution to complex scattering amplitudes $A(\theta)$ and $B(\theta)$ as a function of l. This will help to visualize the subtle differences between the RK and DS approaches.

From Eqs. (19) and (20) it is clear that the partial wave terms within the square brackets should be responsible for the differences found in the results using the RK and DS approaches. We designate the terms in the square brackets in Eqs. (19) and (20) as $A_l(k)$ and $B_l(k)$, respectively. In Figs. 6 and 7 these are plotted as a function of l for p+^{40}Ca at 181 and 362 MeV, respectively. The structures of $\mathrm{Re}A_l(k)$ obtained using both approaches seem to

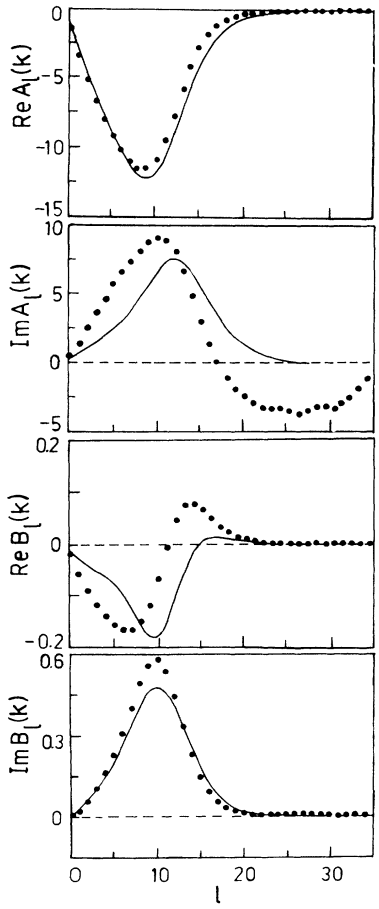

FIG. 6. Plots for $A_l(k)$ and $B_l(k)$ as a function of l for p+^{40}Ca at 181 MeV.

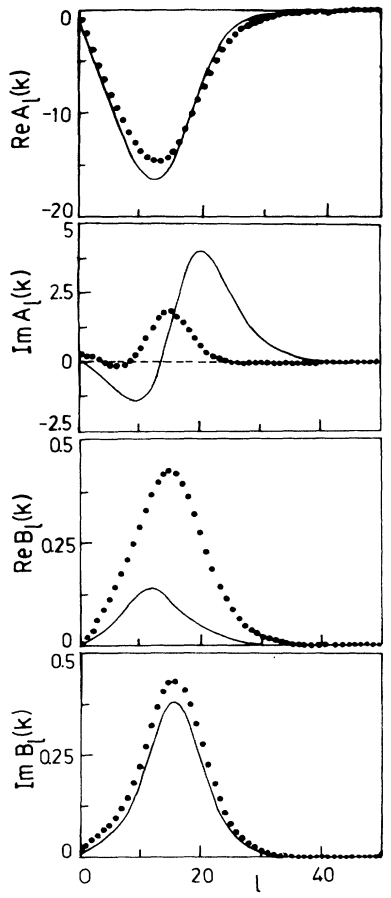

FIG. 7. Same as in Fig. 6 for p+^{40}Ca at E_L = 362 MeV.

be quite similar to each other, whereas there is a significant difference in the structure of $\mathrm{Im}A_l(k)$. More or less the opposite trend is observed for partial wave terms of $B_l(k)$. It is also found that in the DS approach the partial waves which dominate $\mathrm{Re}A_l(k)$ differ from those which dominate $\mathrm{Im}A_l(k)$. This feature is also observed for the case of $B_l(k)$. This essentially implies that a more interesting interference pattern will be generated in using the DS approach in the calculation of spin observables. Structurally speaking, in the DS approach the dominance of different Legendre polynomials in the case of real and imaginary parts of $A(\theta)$ and $B(\theta)$ results in a more intricate interference pattern than one can expect for the case of RK, where both real and imaginary parts of the amplitudes seem to be dominated by approximately the same partial wave. It is found that in general the partial wave amplitudes are highly peaked around the grazing partial wave lg, in both the RK and DS approaches, reflecting the surface dominance.

IV. CONCLUSION

In this paper we have studied the regionwise contribution to the reaction cross section, different facets of the S matrix, and scattering amplitudes. From the regionwise absorption pattern of the partial wave and total absorption cross section, it is found that in both the RK and DS approaches the dominant contribution to the reaction cross section occurs in the surface region. The behavior of $|S_l^{\pm}|$ also reflects this through the fact that it varies rapidly in the surface region, approaching unity for large l. In this sense it is very similar to the low energy heavy ion scattering matrix. But unlike in heavy ion scattering, $|S_l^{\pm}|$ is significantly larger for $l < l_g$ even though surface dominance is the common feature in both. This further substantiates the fact that medium energy relativistic nucleon-nucleus scattering is a surface dominant phenomenon.

The surface dominance of the reaction process leads one to the study of the behavior of partial wave amplitudes as a function of l. It is found that, in general, partial wave amplitude of both $A(\theta)$ and $B(\theta)$ are highly peaked around a partial wave close to the grazing partial wave l_g, and this behavior is also found to be rather symmetric. But some differences between the RK and DS approaches are discernible. In particular we found that in the DS approach, peaking of real and imaginary part of the partial wave amplitudes occurs around different l, indicating that in the results of physical observables generated by this approach a critical role is expected to be played by the interference among slightly differing dominant partial waves.

It is a well-established fact that of the two approaches (namely, the RK and DS), used in the relativistic nucleon-nucleus scattering optical model analysis the DS approach is definitely superior in reproducing the differential cross section and spin observables. In this paper we have given detailed configuration space analysis of the σ_{rec} and the l-space behavior of the amplitudes generated in both of these approaches. Even though both RK and DS approaches can be used to fit the differential cross sections, the σ_{rec} is underestimated in RK but is somewhat overestimated in the DS approach. This is due to the large difference in the strength of the imaginary part of the effective potential used in these approaches. This gives rise to the considerable difference in $|S_l^{\pm}|$ and $\delta_l^{\pm}$ calculated using these two methods. It is seen that one of the primary differences in the RK and DS models is that, for $l < l_g$, the DS model is much more absorptive than is the RK model. Further, the nature of dominance of the real and imaginary parts of partial wave amplitudes in l space generated by the RK and DS methods shows subtle and important differences, even though in general in both cases surface region partial waves are predominant. All the above stated differences play important roles in making the DS method superior in the analysis of intermediate energy proton-nucleus scattering.

ACKNOWLEDGMENTS

The authors gratefully acknowledge the financial assistance in the form of BRNS research Grant No. 37/4/90-G by the Department of Atomic Energy, Government of India for the execution of this work. We also thank Dr. B. Dey for useful discussion and preparation of figures.

[1] L. G. Arnold, B. C. Clark, R. L. Mercer, and P. Schwandt, Phys. Rev. C **23**, 1949 (1981).
[2] D. Frekers *et al.*, Phys. Rev. C **35**, 2236 (1987).
[3] B. C. Clark, S. Hama, and R. L. Mercer, in *Proceedings of the Workshop on the Interaction Between Medium Energy Nucleons in Nuclei*, Indiana University Cyclotron Facility, Bloomington, Indiana, edited by H. O. Meyer, AIP Conf. Proc. No. 97 (AIP, New York, 1983), p. 260.
[4] A. M. Kobos, E. D. Cooper, J. I. Johanson, and H. S. Sherif, Nucl. Phys. **A445**, 605 (1985).
[5] D. L. Pham and R. De Swiniarski, Nuovo Cimento **83A**, 294 (1984).
[6] D. L. Pham and R. De Swiniarski, Nuovo Cimento **103A**, 375 (1990).
[7] R. Kozack and D. G. Madland, Phys. Rev. C **39**, 1461 (1989).
[8] L. Ray, G. W. Hoffman, and W. R. Coker, Phys. Rep. **212**, 224 (1992), and the references therein.
[9] B. C. Clark, S. Hama, R. L. Mercer, L. Ray, and B. D. Serot, Phys. Rev. Lett. **50**, 1644 (1983).
[10] H. Fraunfelder and E. M. Henley, *Subatomic Physics* (Prentice-Hall, Englewood Cliffs, 1974), pp. 234–237.
[11] B. C. Clark, in *Proceedings of the International Symposium on Medium Energy Nucleon and Antinucleon Scat-*

tering, edited by H. V. von Geramb (Springer-Verlag, Berlin, 1985), p. 391.
[12] C. J. Horowitz, Phys. Rev. C **31**, 1340 (1985).
[13] P. P. Murdock and C. J. Horowitz, Phys. Rev. C **35**, 1442 (1987).
[14] S. Hama, B. C. Clark, E. D. Cooper, H. S. Sherif, and R. L. Mercer, Phys. Rev. C **41**, 2737 (1990).
[15] E. D. Cooper, S. Hama, B. C. Clark, and R. L. Mercer, Phys. Rev. C **47**, 297 (1993).
[16] C. S. Shastry and Y. K. Gambhir, Phys. Rev. C **28**, 1109 (1983).
[17] C. S. Shastry and Y. K. Gambhir, Pramana: J. Phys. **23**, 175 (1984).
[18] W. E. Frahn and K. E. Rehm, Phys. Rep. **37**, 1 (1978), and several references cited therein.
[19] C. S. Shastry, J. Phys. G **8**, 1431 (1982).
[20] Y. K. Gambhir and C. S. Shastry, Phys. Rev. C **30**, 1343 (1984).
[21] De Alfaro and T. Regge, *Potential Scattering* (North-Holland, Amsterdam, 1965).
[22] R. G. Newton, *The Complex j-Plane* (Benjamin, New York, 1964).
[23] S. Mukherjee and C. S. Shastry, Nucl. Phys. **B3**, 1 (1967).